




# CircRNA expression profiling and bioinformatics analysis indicate the potential biological role and clinical significance of circRNA in influenza A virus-induced lung injury

JIAJIA WANG<sup>1,†</sup> , YANBING ZHANG<sup>2,†</sup>, FENGFENG ZHU<sup>3</sup>,  
LILING CHEN<sup>4</sup>, YAO WEI<sup>5</sup>, QINGQING ZHU<sup>1</sup>, JUNHONG JIANG<sup>1</sup>,  
JIAN-AN HUANG<sup>1</sup>, QIANG GUO<sup>5\*</sup> and XINJING YANG<sup>5\*</sup>

<sup>1</sup>Department of Pulmonary and Critical Care Medicine, The First Affiliated Hospital of Soochow University, Suzhou 215000, China

<sup>2</sup>Department of General Surgery, The First Affiliated Hospital of Soochow University, Suzhou 215000, China

<sup>3</sup>Department of Emergency and Critical Care Medicine, The Fifth People's Hospital of Suzhou, Suzhou 215000, China

<sup>4</sup>Suzhou Center for Disease Control and Prevention, Suzhou 215004, China

<sup>5</sup>Department of Emergency and Critical Care Medicine, The First Affiliated Hospital of Soochow University, Suzhou 215000, China

\*Corresponding authors (Emails, [ggqq7910@163.com](mailto:ggqq7910@163.com); [yangxinjingsz@163.com](mailto:yangxinjingsz@163.com))

†Jiajia Wang and Yanbing Zhang have equally contributed.

MS received 1 January 2020; accepted 17 February 2021

Circular RNA (circRNA) plays an important role in the regulation of multiple biological processes. However, circRNA profiling and the potential biological role of circRNA in influenza A virus (IAV)-induced lung injury have not been investigated. In the present study, circRNA expression profiles in lung tissues from mice with and without IAV-induced lung injury were analyzed using high-throughput sequencing, and differentially expressed circRNAs were verified by quantitative PCR. The gene homology of candidate circRNAs was investigated and the expression of plasma circRNAs from patients with IAV-induced acute respiratory distress syndrome (ARDS) was detected. The target microRNAs (miRNAs) of circRNAs were predicted. Gene Ontology (GO) and Kyoto Encyclopedia of Genes and Genomes (KEGG) analyses were performed. In total, 781 circRNAs were differentially expressed between ARDS mice and control (467 were up-regulated and 314 were down-regulated). Moreover, the candidate circRNAs (Slco3a1, Nfatc2, Wdr33, and Dmd) expression showed the same trend with the sequencing results. The isoforms of circRNA Slco3a1 and Wdr33 were highly conserved between humans and mice. Plasma circRNA Slco3a1 and Wdr33 presented differential expression in patients with IAV-induced ARDS compared to control. The circRNA-miRNA interaction network and GO and KEGG analyses indicated the potential biological role of circRNAs in the development of IAV-induced lung injury. Taken together, a large number of differentially expressed circRNAs were identified in our study. CircRNA Slco3a1 and Wdr33 had significantly different expression in specimens from mice and humans, and showed a potential biological role in IAV-induced lung injury by bioinformatics analysis.

**Keywords.** circRNA Slco3a1; circRNA Wdr33; miRNA; influenza; lung injury

**Abbreviations:** ARDS, acute respiratory distress syndrome; circRNA, circular RNA; GO, gene ontology; IAV, influenza A virus; KEGG, Kyoto encyclopedia of genes and genomes; miRNA, MicroRNA; qPCR, quantitative PCR.

Electronic supplementary material: The online version contains supplementary material available at <https://doi.org/10.1007/s12038-021-00152-8>.

## 1. Introduction

Acute respiratory distress syndrome (ARDS) is a common complication of influenza A virus (IAV) infection, making it a leading cause of death during influenza epidemic season. The general incidence of ARDS caused by IAV infection is about 2.7 cases per 100000 person-years and accounts for about 4% of hospitalizations due to respiratory failure in influenza epidemic periods (Ortiz *et al.* 2013). Our previous study indicated that ARDS is a leading cause of admission to the intensive care unit and the incidence of ARDS caused by H7N9 virus and H1N1 virus is 58.3% and 27.3%, respectively (Wang *et al.* 2017a). The hospitalization cost and mortality in these patients are significantly higher than those in non-ARDS patients with IAV infection.

The symptoms of ARDS are nonspecific, making it a challenge to distinguish from cardiac pulmonary edema and severe pneumonia. Although therapeutic strategies for ARDS have greatly improved during the past two decades, the general incidence of mortality in patients with moderate and severe ARDS is still more than 40% (Thompson *et al.* 2017). Thus, identifying biomarkers and clarifying the potential mechanism of IAV-induced ARDS could contribute to an early diagnosis, better treatment, and prognostic accuracy.

Circular RNA (circRNA) is a novel type of RNA characterized by covalently closed continuous loops. Gaining a better understanding of the biological roles of circRNA, such as microRNA (miRNA) sponges, RNA-binding protein sequestering agents, and nuclear transcriptional regulators, will provide additional insights into the cellular physiology and disease pathogenesis (Chen 2016). CircRNAs have potential applications as disease biomarkers and novel therapeutic targets in cardiovascular disease, neurological disease, and cancer (Han *et al.* 2018). However, comprehensive circRNA profiling has not been performed in IAV-induced lung injury, and the underlying role of circRNAs is still unknown.

In this study, we investigated the expression profile of circRNA in lung tissues from IAV-infected mice through high-throughput RNA sequencing, and identified a large number of differentially expressed circRNAs between IAV group and control group. The expression of candidate circRNAs was detected in specimens from mice and humans, and bioinformatics analysis was also performed. The results indicate that circRNAs play a potential role in IAV-induced lung injury.

## 2. Materials and methods

### 2.1 Establishment of the mouse model

A/PR/8/34(PR8), a mouse-adapted H1N1 virus strain, has been commonly used for the development of mouse model of influenza A virus-induced lung injury. Here, we used this virus strain as a representative of influenza A virus. Specific pathogen-free male 6-week-old C57B/L6 mice, obtained from the Laboratory Animal Center of Soochow University (Suzhou, China), were anesthetized with 10% chloral hydrate in saline (0.1 mL/10 g) by intraperitoneal injection. Then the mice were challenged intranasally with 15  $\mu$ L  $10^5$  pfu PR8 or phosphate-buffered saline for each nostril. Four days after challenge, the mice were sacrificed by cervical vertebral dislocation. The whole lungs were separated and harvested. The left lungs were fixed in 4% formaldehyde solution for 24 h and then embedded in paraffin. The 5 mm thick sections were stained with hematoxylin and eosin (H&E) and used for lung injury analysis under a microscope. The right lungs were snap frozen in liquid nitrogen and stored at  $-80^{\circ}\text{C}$  for high-throughput RNA sequencing and validation of candidate circRNAs.

### 2.2 High-throughput RNA sequencing of circRNA

Total RNA was isolated using the Hipure Total RNA Mini Kit (Magen, Guangzhou, China) according to the protocol. The concentration and integrity of the total RNA were evaluated by the Qubit 3.0 Fluorometer (Invitrogen, Carlsbad, CA, USA) and Agilent 2100 Bioanalyzer (Applied Biosystems, Carlsbad, CA, USA), respectively. RNA samples with an RNA integrity number value of at least 7.0 or higher were used for further processing. The RNA sequencing library was prepared with approximately 2  $\mu$ g total RNA using the KAPA RNA HyperPrep Kit with RiboErase for Illumina® (Kapa Biosystems, Inc., Woburn, MA, USA). Briefly, ribosomal RNA was removed from the total RNA. The ribosome-depleted RNA was incubated at  $37^{\circ}\text{C}$  for 30 min with 10 units RNase R (Epicentre Technologies, Madison, WI, USA) and purified with VAHTS RNA Clean Beads. Next, ribonucleic RNase R (+) RNAs were fragmented and then first-strand and directional second-strand synthesis were performed. Then A tailing and adapter ligation were performed with the purified cDNA. Finally, the purified, adapter-ligated DNA was amplified. The library quality and concentration were assessed by

utilizing the DNA 1000 chip on the Agilent 2100 Bioanalyzer. Accurate quantification of sequencing applications was determined using the quantitative PCR (qPCR)-based KAPA Biosystems Library Quantification Kit (Kapa Biosystems). Each library was diluted to a final concentration of 10 nM and pooled equimolar prior to clustering. Paired-End (PE150) sequencing was performed on all samples.

### 2.3 Analysis of differentially expressed circRNAs

Differentially expressed circRNAs between the IAV group and control group were screened by using the “edgeR” package in R. Fold change greater than 2.0 and *p* value less than 0.05 were considered statistically significant for differentially expressed circRNAs. A volcano plot with clustering for the differentially expressed circRNAs was constructed with the “gplots” package in R.

### 2.4 Detection of candidate circRNAs

Six circRNAs in mouse lung tissues from the top 20 differentially expressed circRNAs were selected for further validation using qPCR in 10 specimens (5 specimens in each group), and the predicted human

conserved circRNAs were also tested in human plasma (5 specimens for each group). The total RNA was extracted with TRIzol® Reagent (Invitrogen) and reverse-transcribed to synthesize first-strand cDNA with the Genesee® II First Strand cDNA Synthesis Kit (Genesee, Guangzhou, China). Then qPCR was performed with the Applied Biosystems 7500 Real-Time PCR system. The housekeeping genes  $\beta$ -actin and U6 were used as controls and the relative expression of circRNAs was calculated with the  $2^{-\Delta\Delta CT}$  method. The specific primers for these candidate circRNAs were designed (table 1).

### 2.5 Prediction of human conserved circRNAs

LiftOver tool (<http://genome.ucsc.edu/cgi-bin/hgLiftOver>) was used to identify human conserved circRNAs (parameters:-bedPlus = 3-tab-minMatch = 0.1-minBlocks =1). We first investigated the back-splicing site of a circRNA and obtained the corresponding location in the mouse genome. If the corresponding human genome was located at the back-splicing site of the circRNA in the circbase database, the circRNA was considered conservative, and then the ID number of the circbase was made available. The homology comparison between mice and humans was

**Table 1.** Primer sequences for each gene

Genes name	circbase ID	Primers	Sequences	Product length (bp)
Slco3a1	mmu_circ_0014392	Forward	5'-CAGCCACGAACATGATGTACT-3'	149
		Reverse	5'-GTCAACACGCTCACCTATGT-3'	
	hsa_circ_0003252	Forward	5'-CCTCGCTCTATATAGGTGAG-3'	118
		Reverse	5'-AGAGGATGAGCGCCAGGTTTC-3'	
Fam53b	mmu_circ_0013952	Forward	5'-GCCAAGATGGCACAGAAAATGA-3'	173
		Reverse	5'-GTCTTTGATTAGGCTGGTCAC-3'	
Sept9	mmu_circ_0002788	Forward	5'-AGCTGAGGCACCCAACTGTC-3'	143
		Reverse	5'-ACGATCTCTTTAAGGCTTCC-3'	
Nfatc2	mmu_circ_0009613	Forward	5'-CCCTGTGGTGCAGAACCTCT-3'	148
		Reverse	5'-AAAGCCTCTGCGCACGAATG-3'	
Wdr33	mmu_circ_0000858	Forward	5'-GGAAAGAATTCTCCGAGTGACT-3'	172
		Reverse	5'-ATCAAAGGTGAGCTGCTGCATT-3'	
	hsa_circ_0003192	Forward	5'-CAGTTTCTCACCCACGGATA-3'	116
		Reverse	5'-TTTCCTTCTAGGATACTCGG-3'	
Dmd	mmu_circ_0016387	Forward	5'-CAGATAGCAGTCAGCCTATG-3'	165
		Reverse	5'-GACGAGGCAGGCCTTTGAA-3'	
$\beta$ -actin		Forward	5'-GCTTCTAGGCGGACTGTTAC-3'	100
		Reverse	5'-CCATGCCAATGTTGTCTCTT-3'	
U6		Forward	5'-CTCGCTTCGGCAGCACA-3'	94
		Reverse	5'-AACGCTTCACGAATTTGCGT-3'	

performed with the Basic Local Alignment Search Tool (<https://blast.ncbi.nlm.nih.gov/Blast.cgi>).

### 2.6 Prediction of target miRNAs for candidate circRNAs and the functional analysis

The miRanda databases were used to identify the possible binding of miRNAs with circRNAs. The main criteria for predicting a possible circRNA-miRNA interaction including sequence matching, thermal stability (free energy) of double-stranded binding of miRNA-circRNA, and conservativeness of target sites. The predicted miRNAs with a total score > 140 and total energy < -20 were enrolled in our study. All miRNA gene targets were identified with a  $p < 0.05$ . The networks between circRNAs and miRNAs were built with Cytoscape and the miRNAs with the top 10 total scores were enrolled in the networks. Gene Ontology (GO) analysis (<http://geneontology.org/>) was performed to predict the potential function of circRNAs in terms of biological process, cellular components, and molecular functions. Kyoto Encyclopedia of Genes and Genomes (KEGG) analysis (<http://www.genome.jp/kegg/>) was also performed to further explore the signaling pathways of circRNA-related target genes. The significance threshold was classified as  $p < 0.05$  and FDR value < 0.01.

### 2.7 Collection of patient plasma and ethical statement

Patients with IAV-induced ARDS and paired healthy individuals were enrolled in our study. Peripheral blood from all participants (6 mL) was collected in an EDTA tube and stored at 4°C for less than 1 h. The blood should be centrifuged within 1 h at  $3000 \times g$  for 15 min to obtain plasma, and then stored at -80°C. This study was approved by the Institutional Review Board of the First Affiliated Hospital of Soochow University, and informed consents were obtained from all participants.

### 2.8 Statistical analysis

All values were presented as the mean  $\pm$  standard deviation. The difference between two groups was evaluated by the independent samples *t*-test. All of the statistical analyses were performed using SPSS 22.0 software package and visualized by Graphpad

Prism 5.0. A  $p < 0.05$  was considered statistically significant.

## 3. Results

### 3.1 CircRNA expression profiling and the distribution of differentially expressed circRNAs in mouse chromosomes

Pathological features of lung tissues from IAV-infected mice were characterized by serious alveolar collapse and consolidation, significant alveolar congestion and hemorrhage, and extensive inflammatory cell infiltration (figure 1A). Lung tissue from the control group indicated normal lung histology (figure 1B). Compared to the control group, circRNA expression in lung tissue from IAV-infected mice presented a greater than two-fold change and  $p < 0.05$  were considered biologically meaningful. In total, 781 differentially expressed circRNAs were identified, of which 467 were significantly up-regulated and 314 were down-regulated (figure 1C). Read statistics (Table S1) and read quality plot (supplementary figure 1) of next-generation sequencing have been given as supplementary data. Volcano plots were used to visualize differentially expressed circRNAs between the two groups (figure 1D). Furthermore, the top 20 up-regulated and 20 down-regulated circRNAs were listed according to fold change in expression (table 2). We also investigated the distribution of differentially expressed circRNAs in mice chromosomes. The circular plot indicated differentially expressed circRNAs located in almost all mice chromosomes, except chromosome Y (supplementary figure 2A). The circRNAs were mostly located on chromosomes 2 and 5 (64 for each chromosome). The up-regulated circRNAs were mostly located on chromosome 5 and the down-regulated circRNAs were mostly located on chromosomes 2 and 9 (supplementary figure 2B).

### 3.2 Validation of candidate circRNAs and the gene homology analysis of differentially expressed circRNAs

Four up-regulated (circRNA Slco3a1, Fam53b, Sept9, and Nfatc2) and two down-regulated (circRNA Wdr33 and Dmd) circRNAs from the table 2 were selected for further analysis by qPCR in 10 lung tissues (5 samples for each group). The results showed that circRNA Slco3a1 and circRNA Nfatc2 were significantly up-regulated in lung tissues from IAV-infected mice compared with the control group, and circRNA Wdr33

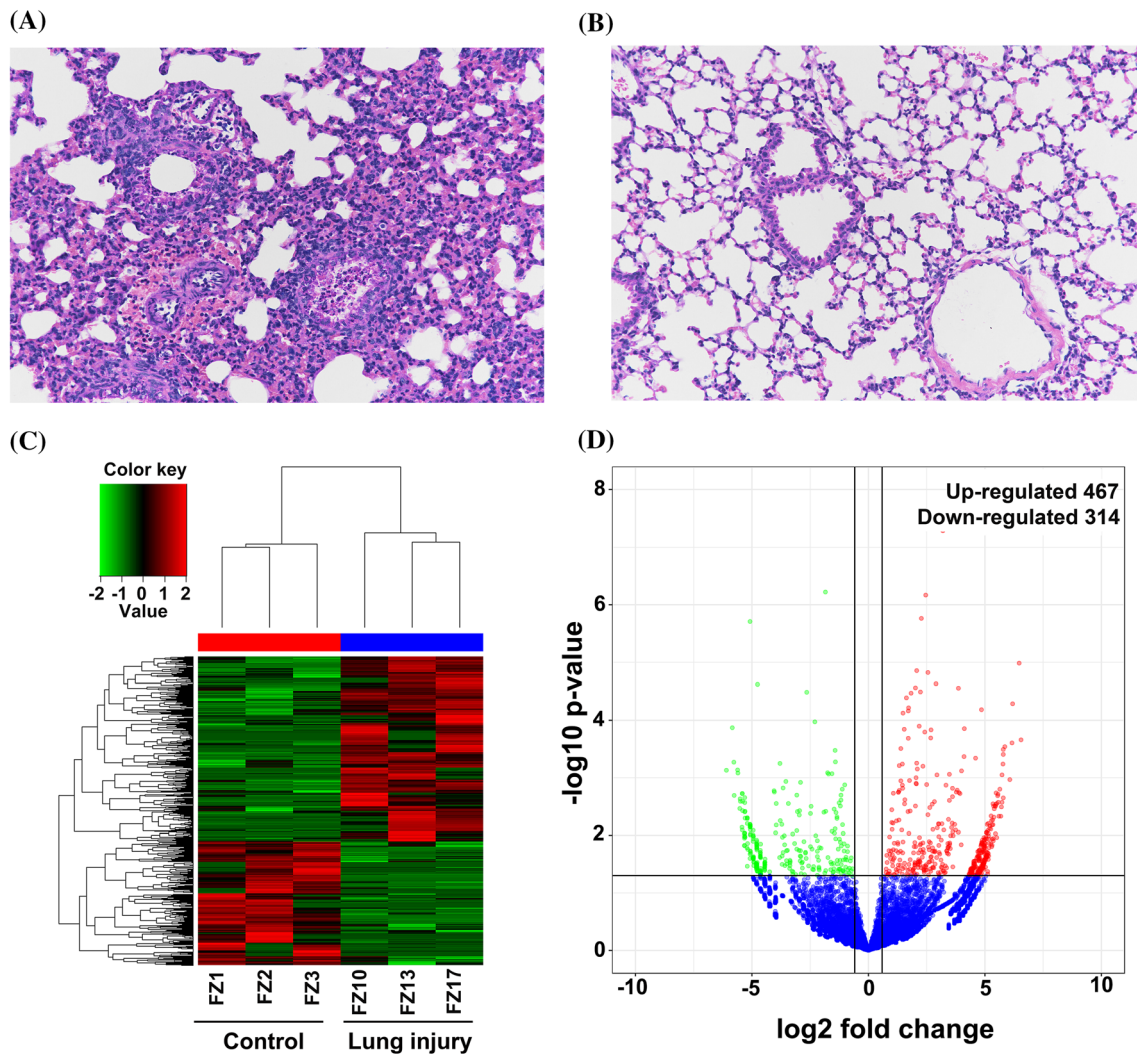


**Figure 1.** Comprehensive circRNA profiling in lung tissues from mice with and without IAV-induced lung injury. (A) H&E staining (200 $\times$ ) of lung tissue from mice with IAV-induced lung injury. (B) H&E staining (200 $\times$ ) of lung tissue from control mice. (C) The heat map indicates the differential expression of circRNAs between two groups (3 samples for each group). The high and low expression of circRNAs are marked in red and green, respectively. (D) Volcano plots of circRNA expression. The two vertical lines represent the differential expression of 2-fold up and down, and the horizontal line represents  $p=0.05$ . Thus, the green dots demonstrate the low expression with statistical difference, and the red dots demonstrate high expression with statistical difference.

and circRNA Dmd were significantly down-regulated (figure 2A). Among the 781 differentially expressed circRNAs in mice, 323 were confirmed to be conserved in humans (41.36%). Furthermore, we found 192 human conserved circRNAs in 467 up-regulated circRNAs (41.11%) and 131 human conserved circRNAs in 314 down-regulated circRNAs (41.72%) (figure 2B). Specifically, we found that the circRNA Slco3a1 isoform located on chr7\_74504176\_74504642 in the mouse genome (mmu\_circ\_0014392) and chr15\_92459222\_92459688 in the human genome (hsa\_circ\_0003252) were highly conserved with identities of 88% (supplementary figure 3A). CircRNA

Wdr33 isoform located on chr18\_31827261\_31835481 in the mouse genome (mmu\_circ\_0000858) and chr2\_128520635\_128528578 in the human genome (hsa\_circ\_0003192) were highly conserved with identities of 93% (supplementary figure 3B).

### 3.3 CircRNA-miRNA interaction networks and the expression level of human plasma circRNA Slco3a1 and circRNA Wdr33

We constructed circRNA-miRNA interaction networks for all differentially expressed circRNAs

**Table 2.** The top 20 upregulated and top 20 downregulated circRNAs in lung tissues from mice with IAV-induced lung injury

Gene	mmu_circbase_id	Fold change	Difference	P value
Nab1	mmu_circ_0008772	28.856	up	0.000
Ambra1	mmu_circ_0001046	12.245	up	0.002
Slco3a1	mmu_circ_0014392	9.205	up	0.000
Zfp516	mmu_circ_0007569	8.909	up	0.036
Fam53b	mmu_circ_0013952	7.454	up	0.000
Rbbp4	mmu_circ_0011224	6.825	up	0.008
Copb1	mmu_circ_0001615	6.75	up	0.019
Vps54	mmu_circ_0002874	6.658	up	0.003
Galnt7	mmu_circ_0014869	6.475	up	0.023
Zkscan1	mmu_circ_0012225	6.348	up	0.014
Cryl1	mmu_circ_0000543	6.229	up	0.029
Usp12	mmu_circ_0012340	6.185	up	0.003
Lats2	mmu_circ_0005309	5.894	up	0.000
Nfatc2	mmu_circ_0001103	5.528	up	0.000
4933426M11Rik	mmu_circ_0004228	5.228	up	0.02
Sept9	mmu_circ_0002788	5.0456	up	0.001
Slc10a7	mmu_circ_0014994	4.977	up	0.024
Nfatc2	mmu_circ_0009613	4.847	up	0.000
Lphn3	mmu_circ_0012809	4.5981	up	0.028
Tor1a	mmu_circ_0009821	4.567	up	0.011
Mlip	mmu_circ_0001809	-33.767	down	0.000
Hace1	mmu_circ_0002239	-16.502	down	0.002
Ptpla	mmu_circ_0009382	-13.949	down	0.001
Ptk2	mmu_circ_0005767	-12.103	down	0.015
Poc1b	mmu_circ_0002616	-11.664	down	0.001
Tbcd	mmu_circ_0002854	-9.439	down	0.043
Gdap2	mmu_circ_0010973	-8.643	down	0.048
Wdr33	mmu_circ_0000858	-8.243	down	0.004
Ascc2	mmu_circ_0003047	-7.558	down	0.001
Akap7	mmu_circ_0000153	-6.783	down	0.013
Gli3	mmu_circ_0004514	-6.707	down	0.048
Bmpr1b	mmu_circ_0010499	-5.9436	down	0.034
Atf7ip	mmu_circ_0013135	-5.336	down	0.017
Pcmt1	mmu_circ_0002393	-5.089	down	0.035
Arid2	mmu_circ_0006009	-4.794	down	0.01
Dmd	mmu_circ_0016387	-4.576	down	0.024
Arhgap32	mmu_circ_0001764	-3.604	down	0.000
Cdk8	mmu_circ_0012324	-3.553	down	0.004
Boc	mmu_circ_0006305	-3.36	down	0.001
Gfra1	mmu_circ_0007972	-3.287	down	0.001

(supplementary figure 4). We also constructed circRNA-miRNA interaction networks for circRNA Slco3a1 and Wdr33. The 10 highest ranking target miRNAs for each circRNA isoform were enrolled in the networks (figure 3A–D). The relative expression of plasma circRNA Slco3a1 and circRNA Wdr33 in ARDS patients was quantified with qPCR technology. CircRNA Slco3a1 was significantly up-regulated and circRNA Wdr33 was significantly down-regulated in ARDS patients compared to control (figure 3E, F).

### 3.4 GO and KEGG analyses of circRNA Slco3a1 and Wdr33 in mice and humans

Biological process analysis demonstrated that the isoforms of circRNA Slco3a1 and Wdr33 in mice and humans were mainly involved in synthesis and metabolism of biomolecules, mitochondrial function, and superoxide metabolic process (figures 4A, 5A). Cellular components analysis of circRNA Slco3a1 and Wdr33 showed their target genes were mainly implicated in mitochondria and/or Golgi apparatus

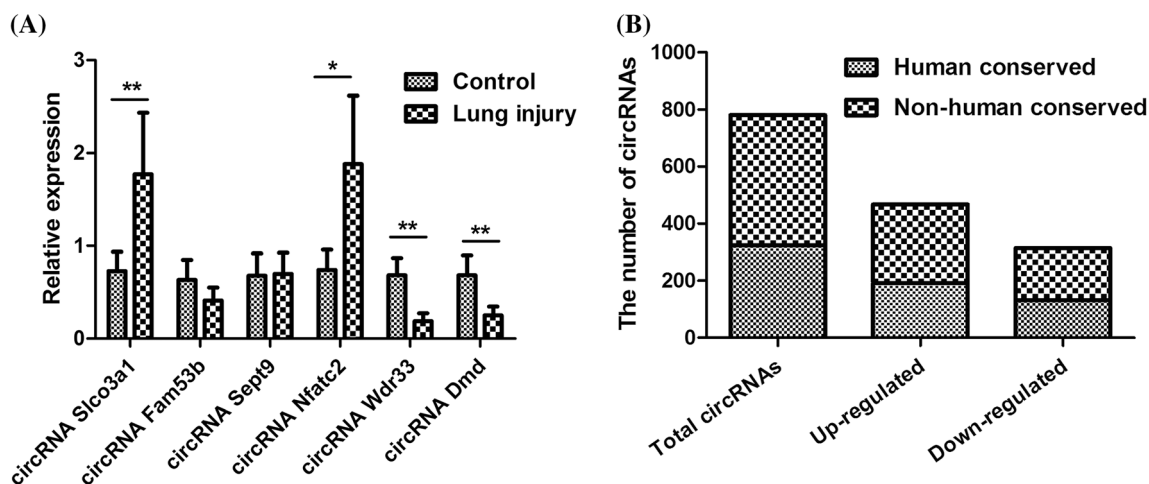


**Figure 2.** Validation of candidate circRNAs with qPCR and the homology analysis of differentially expressed circRNAs. (A) Candidate circRNAs presented differential expression with statistical significance. Comparison was made by Independent sample t-tests (\*  $p < 0.05$ , \*\*  $p < 0.01$ ). (B) The number of human conserved circRNAs in mice with IAV-induced lung injury.

(figures 4B, 5B). Molecular functions analysis of these two circRNAs showed their target genes were mainly enriched in terms of enzyme activity regulation such as cofactor binding, coenzyme binding, and peptidase regulator activity (figures 4C, 5C). KEGG analysis revealed that the main pathways related to the isoforms of circRNA Slco3a1 and Wdr33 in mice were carbon metabolism, hippo signaling pathway, and oxidative phosphorylation (figure 4D). However, the signaling pathways of the isoforms of circRNA Slco3a1 and Wdr33 in humans were mainly associated with pathogen infection, the c-type lectin receptor signaling pathway, and notch signaling pathway (figure 5D).

#### 4. Discussion

In the present study, we investigated circRNA profiling in mice with IAV-induced lung injury using high-throughput RNA sequencing, and found abundant differentially expressed circRNAs. The differential expression of candidate circRNAs was validated in mice lung tissues, and also confirmed in plasma from ARDS patients with IAV infection by qPCR technology. The interaction networks between circRNAs and their target miRNAs were constructed. In addition, GO and KEGG analyses were also performed, from which the potential biological role and clinical significance of circRNAs in the development of IAV-induced lung injury were preliminarily demonstrated.

Circular RNAs, a novel class of noncoding RNAs characterized by covalently closed continuous loops

without 5'-3' polarity and a polyadenylated tail, play an important role in the genetic regulation of multiple biological process (Salzman 2016). They have features of high abundance and stability, are evolutionarily conserved among species, and are expressed in a tissue-specific manner and pathology-specific context, indicating their potential applications as suitable biomarkers and novel therapeutic targets (Qu *et al.* 2015).

ARDS is a common complication in clinical settings and is also a life-threatening form of respiratory failure in critically ill patients. ARDS most often develops in the context of pneumonia (such as bacterial and viral) and sepsis (Matthay *et al.* 2019). Since the high morbidity and mortality remain major challenges in the management of ARDS patients, basic research on ARDS development would be beneficial for preventing or treating this disease (Fan *et al.* 2018). To date, little is known about the role of circRNAs in the pathophysiological process of ARDS. In a previous study, the expression profiles of circRNAs were analyzed in lung tissues from rats with LPS-induced ARDS and a large number of differentially expressed circRNAs was found (Wan *et al.* 2017). In another study, comprehensive circular RNA profiling in LPS-induced acute lung injury mice preliminarily demonstrated aberrantly expressed circRNAs and the potential molecular mechanism (Li *et al.* 2019b). In the current study, we first investigated the expression profiles of circRNAs in mice with IAV-induced lung injury and found a large number of circRNAs expressed in a pathology-specific manner.

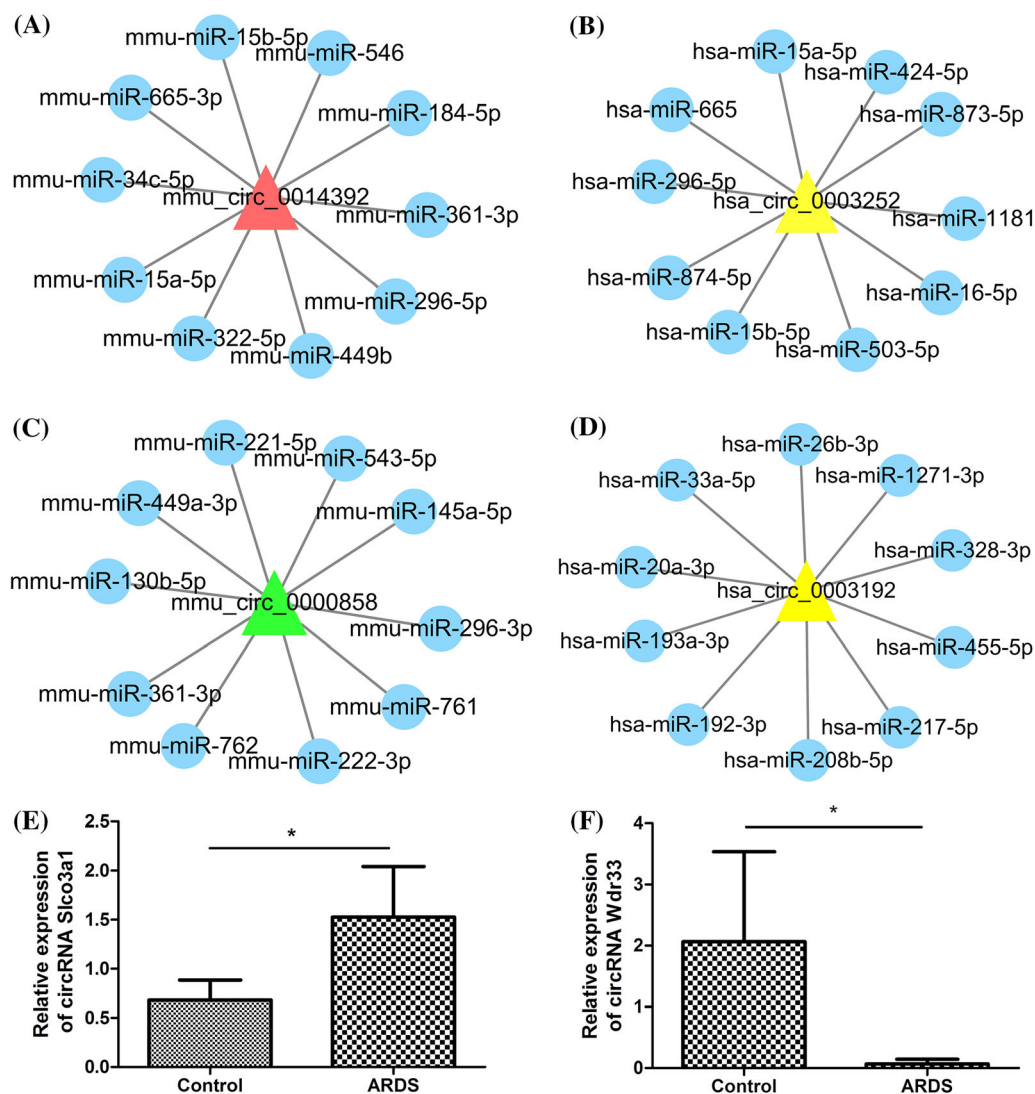


**Figure 3.** Prediction of target miRNAs for candidate circRNAs, and the expression level of circRNA *Slco3a1* and circRNA *Wdr33* in plasma. The triangle represents circRNAs and the round represents miRNAs. (A) CircRNA *Slco3a1* isoform (*mmu\_circ\_0014392*) and its target miRNAs. (B) CircRNA *Slco3a1* isoform (*hsa\_circ\_0003252*) and its target miRNAs. (C) CircRNA *Wdr33* isoform (*mmu\_circ\_0000858*) and its target miRNAs. (D) CircRNA *Wdr33* isoform (*hsa\_circ\_0003192*) and its target miRNAs. (E) CircRNA *Slco3a1* was significantly up-regulated in ARDS patients. (F) CircRNA *Wdr33* was significantly down-regulated in ARDS patients.

Approximately 5–30% of circRNAs are completely conserved in closely related species such as humans and mice. In our study, we found 41.36% of human conserved circRNAs in differentially expressed circRNAs in mice. As two circRNA isoforms of gene *Slco3a1* and *Wdr33*, *mmu\_circ\_0014392* and *hsa\_circ\_0003252*, *mmu\_circ\_0000858* and *hsa\_circ\_0003192* were highly conserved. CircRNA *Slco3a1* and circRNA *Wdr33* were aberrantly expressed in the lung tissues of the ARDS animal model and plasma from ARDS patients, indicating the potential role of circRNA *Slco3a1* and circRNA *Wdr33* in the development of IAV-induced ARDS.

It has been reported that circRNAs can regulate gene expression through the regulation of transcription and alternative splicing, interaction with RNA-binding proteins, miRNA sponge, and even translation (Han *et al.* 2018). Among these mechanism of genetic regulation, the functions of acting as miRNA sponges or competitive endogenous RNAs have garnered great attention (Rossbach 2019). In this study, the circRNA-miRNA interaction network was established and a possibly extensive interaction between circRNAs and miRNAs was predicted. After reviewing the literature on these target miRNAs, we found that some are reportedly involved in virus infection



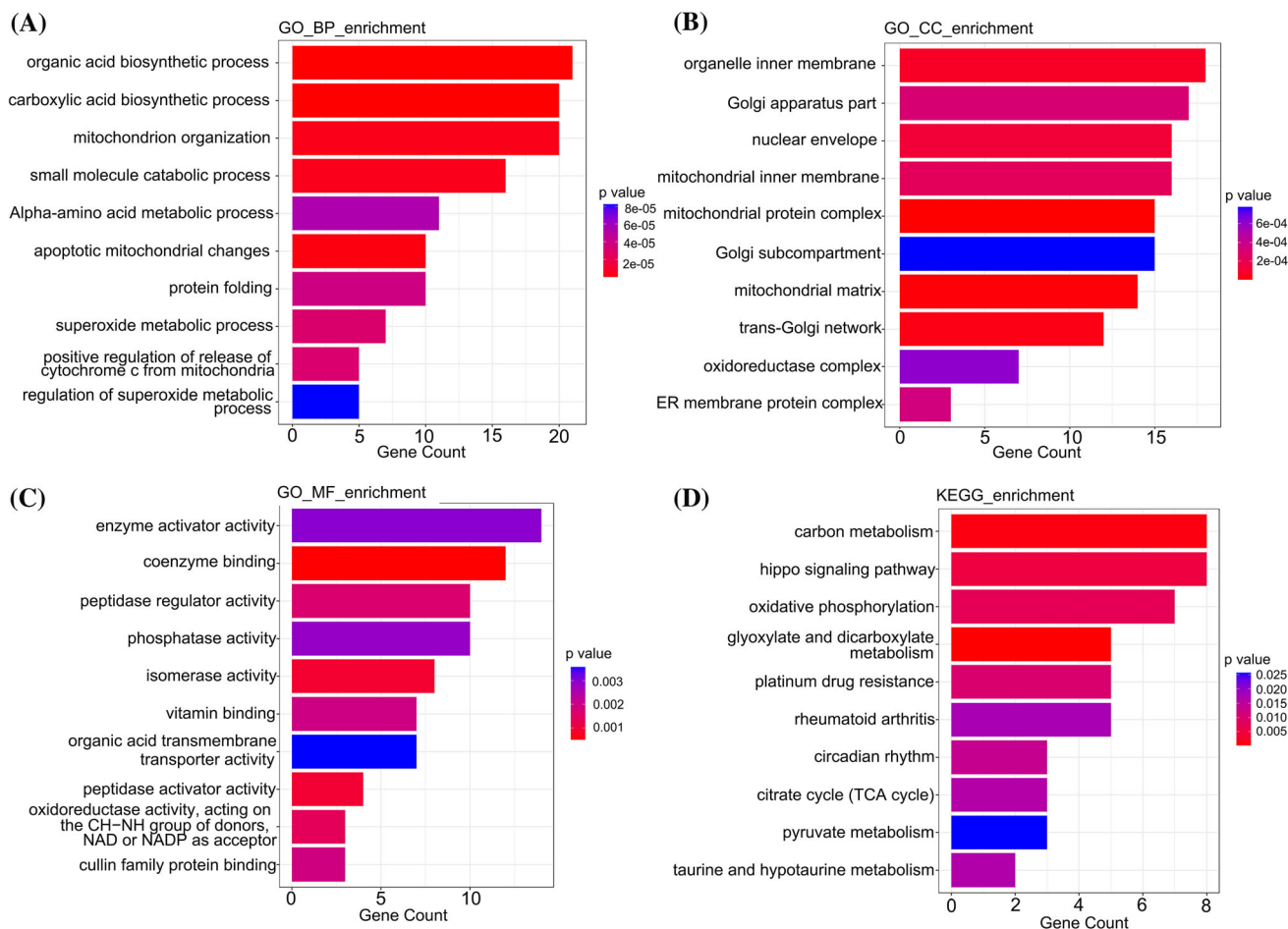


**Figure 4.** Functional annotation of circRNA Slco3a1 and circRNA Wdr33 in mice. The columns listed in GO and KEGG analyses indicate the top 10 significant enrichment. (A) Biological process analysis; (B) Cellular components analysis; (C) Molecular functions analysis; (D) KEGG pathway analysis.

and/or inflammation regulation. As predicted, the target miRNA of circRNA Slco3a, miRNA-15b, is involved in Japanese encephalitis virus infection and can alleviate high glucose-induced cell apoptosis, oxidative stress, and inflammatory responses (Zhu *et al.* 2016; Fu *et al.* 2019; Shen *et al.* 2019). It has been reported that miRNA-16 can alleviate lipopolysaccharide (LPS)-induced A549 cell injury, inhibit NLRP3 inflammasome activation, and suppress enterovirus 71 replication (Zheng *et al.* 2017; Liu *et al.* 2019; Yang *et al.* 2019). As target miRNAs of circRNA Wdr33, miRNA-543 and miRNA-130b are reportedly involved in the regulation of ameliorating inflammatory injury in multiple pathophysiological processes (Wang *et al.* 2017b; Zheng *et al.* 2018; Zhao *et al.* 2019). To further investigate the biological role of those target genes contained in the circRNA-miRNA network, we also performed GO and KEGG analyses. Biological process analysis revealed that circRNA Slco3a1 and Wdr33 might be

involved in mitochondrial function and superoxide metabolic process. Superoxide and mitochondrial dysfunction are associated with inflammatory response, alveolar epithelial cells apoptosis, and lung barrier impairment (Liu *et al.* 2014; Song *et al.* 2016). Furthermore, KEGG analysis showed that signaling pathways, such as the hippo signaling pathway, oxidative phosphorylation, and notch signaling pathway, had a close relationship with lung injury (Li *et al.* 2015, 2019a, 2020). These bioinformatics analyses provide insights into the vital regulatory role of circRNA Slco3a1 and circRNA Wdr33 in the development of IAV-induced lung injury. It is notable that KEGG analysis revealed different signaling pathways in mice and humans, indicating the complex regulatory mechanism of circRNA in different species. It has been confirmed that circRNA GATAD2A can promote H1N1 virus replication by inhibiting autophagy. However, to date, comprehensive profiling and the potential role of circRNA in

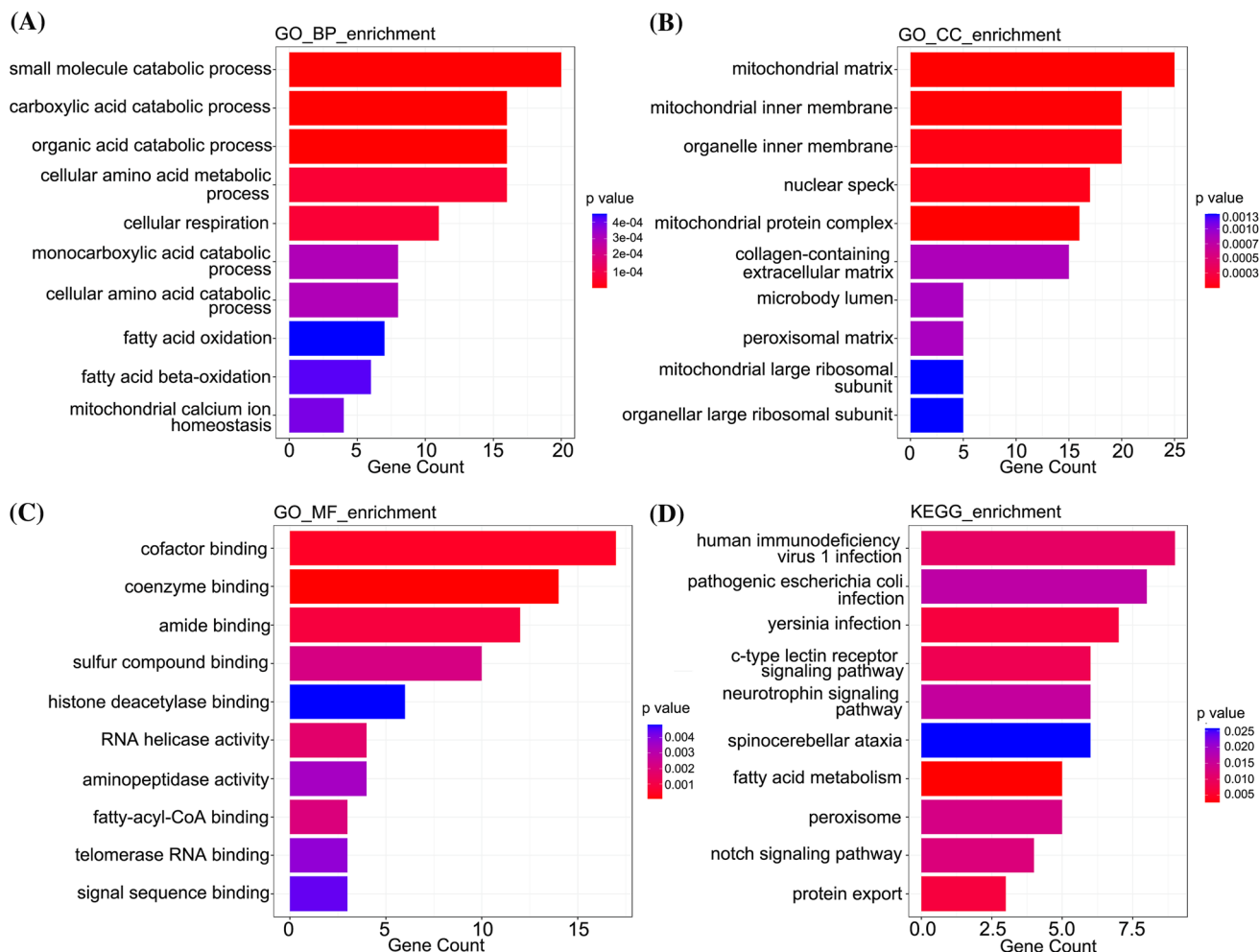


**Figure 5.** Functional annotation of circRNA Slco3a1 and circRNA Wdr33 in humans. The columns listed in GO and KEGG analyses indicate the top 10 significant enrichment. (A) Biological process analysis; (B) Cellular components analysis; (C) Molecular functions analysis; (D) KEGG pathway analysis.

IAV-induced lung injury has not been explored (Yu et al. 2019).

In conclusion, this is the first study to explore the expression profile of circRNAs in IVA-induced lung injury. After the detection of candidate circRNAs in specimens from both mice and humans, gene homology analysis, construction of circRNAs and miRNAs interaction networks, and GO and KEGG analyses, we found the potential biological role and clinical significance of circRNAs in IAV-induced lung injury. Additional studies are needed to reveal the function and underlying mechanism of circRNA Slco3a1 and circRNA Wdr33 in IAV-induced lung injury.

## Acknowledgements

This work was supported by grants from the National Science and Technology Major Project (No.

2017ZX10204401003), the Suzhou Science and Technology Project (Nos. KJXW2018008, SYS2019048, and SS201711), and the Suzhou Medical Key Subject (SZXK201516). We would like to thank Dr. Anushka Aghi, from Panchkula, India, for her help in the development of this manuscript.

**Ethical approval** This study was approved by the Institutional Review Board of the First Affiliated Hospital of Soochow University, and informed consents were obtained from all participants.

## References

- Chen LL 2016 The biogenesis and emerging roles of circular RNAs. *Nat. Rev. Mol. Cell Biol.* **17** 205–211
- Fan E, Brodie D and Slutsky AS 2018 Acute respiratory distress syndrome: advances in diagnosis and treatment. *JAMA* **319** 698–710

- Fu Y, Wang C, Zhang D, Chu X, Zhang Y and Li J 2019 miR-15b-5p ameliorated high glucose-induced podocyte injury through repressing apoptosis, oxidative stress, and inflammatory responses by targeting Sema3A. *J. Cell. Physiol.* **234** 20869–20878
- Han B, Chao J and Yao H 2018 Circular RNA and its mechanisms in disease: From the bench to the clinic. *Pharmacol. Therapeut.* **187** 31–44
- Li KC, Ho YL, Hsieh WT, Huang SS, Chang YS and Huang GJ 2015 Apigenin-7-glycoside prevents LPS-induced acute lung injury via downregulation of oxidative enzyme expression and protein activation through inhibition of MAPK phosphorylation. *Int. J. Mol. Sci.* **16** 1736–1754
- Li L, Dong L, Gao F, Hui J, Chen Y and Yan J 2019a Effects of Hippo signaling pathway on lung injury repair by mesenchymal stem cells in acute respiratory distress syndrome. *Zhonghua Wei Zhong Bing Ji Jiu Yi Xue* **31** 281–287
- Li X, Yuan Z, Chen J, Wang T, Shen Y and Chen L 2019b Microarray analysis reveals the changes of circular RNA expression and molecular mechanism in acute lung injury mouse model. *J. Cell Biochem.* **120** 16658–16667
- Li M, Zhao Y, Qi D, He J and Wang D 2020 Tangeretin attenuates lipopolysaccharide-induced acute lung injury through Notch signaling pathway via suppressing Th17 cell response in mice. *Microb. Pathog.* **138** 103826
- Liu G, Zhang J, Chen H, Wang C, Qiu Y, Liu Y, Wan J and Guo H 2014 Effects and mechanisms of alveolar type II epithelial cell apoptosis in severe pancreatitis-induced acute lung injury. *Exp. Ther. Med.* **7** 565–572
- Liu GP, Wang WW, Lu WY and Shang AQ 2019 The mechanism of miR-16-5p protection on LPS-induced A549 cell injury by targeting CXCR3. *Artif. Cells Nanomed. Biotechnol.* **47** 1200–1206
- Matthay MA, Zemans RL, Zimmerman GA, Arabi YM, Beitler JR, Mercat A, Herridge M, Randolph AG and Calfee CS 2019 Acute respiratory distress syndrome. *Nat. Rev. Dis. Primers* **5** 18
- Ortiz JR, Neuzil KM, Rue TC, Zhou H, Shay DK, Cheng PY, Cooke CR and Goss CH 2013 Population-based Incidence Estimates of Influenza-associated Respiratory Failure Hospitalizations 2003 to 2009. *Am. J. Respir. Crit. Care Med.* **188** 710–715
- Qu S, Yang X, Li X, Wang J and Li H 2015 Circular RNA: a new star of noncoding RNAs. *Cancer Lett.* **365** 141–148
- Rosbach O 2019 Artificial circular RNA sponges targeting microRNAs as a novel tool in molecular biology. *Mol. Therapy Nucleic Acids* **17** 452–454
- Salzman J 2016 Circular RNA expression: its potential regulation and function. *Trends Genet.* **32** 309–316
- Shen H, Fang K, Guo H and Wang G 2019 high glucose-induced apoptosis in human kidney cells was alleviated by miR-15b-5p mimics. *Biol. Pharm. Bull.* **42** 758–763
- Song MJ, Davidovich N, Lawrence GG and Margulies SS 2016 Superoxide mediates tight junction complex dissociation in cyclically stretched lung slices. *J. Biomech.* **49** 1330–1335
- Thompson BT, Chambers RC and Liu KD 2017 Acute respiratory distress syndrome. *New Engl. J. Med.* **377** 562–572
- Wan QQ, Wu D and Ye QF 2017 The expression profiles of circRNAs in lung tissues from rats with lipopolysaccharide-induced acute respiratory distress syndrome: A microarray study. *Biochem. Biophys. Res. Commun.* **493** 684–689
- Wang J, Xu H, Yang X, Zhao D, Liu S, Sun X, Huang JA and Guo Q 2017a Cardiac complications associated with the influenza viruses A subtype H7N9 or pandemic H1N1 in critically ill patients under intensive care. *Braz. J. Infect. Dis.* **21** 12–18
- Wang P, Zhang X, Li F, Yuan K, Li M, Zhang J, Li B and Liang W 2017b MiR-130b attenuates vascular inflammation via negatively regulating tumor progression locus 2 (Tpl2) expression. *Int. Immunopharmacol.* **51** 9–16
- Yang Y, Yang F, Yu X, Wang B, Yang Y, Zhou X, Cheng R, Xia S and Zhou X 2019 miR-16 inhibits NLRP3 inflammasome activation by directly targeting TLR4 in acute lung injury. *Biomed. Pharmacother.* **112** 108664
- Yu T, Ding Y, Zhang Y, Liu Y, Li Y, Lei J, Zhou J, Song S and Hu B 2019 Circular RNA GATAD2A promotes H1N1 replication through inhibiting autophagy. *Vet Microbiol.* **231** 238–245
- Zhao CL, Cui HA and Zhang XR 2019 MiR-543-5p inhibits inflammation and promotes nerve regeneration through inactivation of the NF-kappaB in rats after spinal cord injury. *Eur Rev Med. Pharmacol. Sci.* **23** 39–46
- Zheng C, Zheng Z, Sun J, Zhang Y, Wei C, Ke X, Liu Y, Deng L and Wang H 2017 MiR-16-5p mediates a positive feedback loop in EV71-induced apoptosis and suppresses virus replication. *Sci. Rep.* **7** 16422
- Zheng DZ, Bu YM and Wang L 2018 miR-130b participates in wear particle-induced inflammation and osteolysis via FOXF2/NF-kappaB pathway. *Immunopharmacol. Immunotoxicol.* **40** 408–414
- Zhu B, Ye J, Ashraf U, Li Y and Cao S 2016 Transcriptional regulation of miR-15b by c-Rel and CREB in Japanese encephalitis virus infection. *Sci. Rep.* **6** 22581